Robust extended-range wireless power transfer using a higher-order PT-symmetric platform

Maryam Sakhdari, Mehdi Hajizadegan, and Pai-Yen Chen [*]

Department of Electrical and Computer Engineering, University of Illinois at Chicago, Chicago, Illinois 60607, USA

A fundamental challenge for the nonradiative wireless power transfer (WPT) resides in maintaining the stable power transmission with a consistently high efficiency under dynamic conditions. Here, we propose and experimentally demonstrate that a frequency-locked WPT system satisfying the higher-order parity-time (PT) symmetry can achieve a near-unity power transfer efficiency that is resilient to effects of distance variation and misalignment between coils, and impedance fluctuations in electric grids. In specific higher-order PT electronic systems, a purely real-valued and coupling-invariant (nonbifurcated) eigenfrequency would enable the robust and efficient wireless charging without frequency hopping or adaptive impedance matching, even for midrange operation. We envision that this WPT technique may provide reliable, fast and efficient power delivery for a variety of consumer electronics, electric vehicles, and medical devices.

I. INTRODUCTION

Radio-frequency (RF) wireless power transfer (WPT) has experienced a rapid and widespread growth in recent years, as driven by the rising demand for wireless charging in consumer electronics, medical devices, sensors, and automotive applications [1–10]. The concept of transferring power without any physical contact was put forward soon after the proposition of Faraday's law of induction [11]. In late 1890s, Nikola Tesla conducted pioneering experiments with lighting electric bulbs wirelessly through electrodynamic induction (also known as resonant inductive coupling) [12]. Although his efforts appear to have met with little success, nowadays, considerable progress in WPT has been made in the realm of nonradiative transfer that employs the near-field magnetic coupling to efficiently transmit electrical energy from a power source to electrical loads [3]. While the WPT technology has motivated considerable research and development in the past two decades [13–15], there are still several fundamental issues which need further investigation to maximize the potential of this technology. Traditional WPT systems are not robust against alteration of distance and misalignment between coils [5,16], and variations in the terminating impedance of an electric power grid or battery over time [1]. To date, several techniques have been proposed to optimize the efficiency of power transfer, which include dynamic adjustment of operating frequency (resonant-frequency tracking) [17,18], combination of multiple receivers and repeaters for adaptive impedance matching [19], and adding nonlinear tuning elements in circuits [7,10]. For these often used WPT schemes,

when the coupling factor (as a function of distance and alignment between coils) changes, the operating frequency must be adjusted accordingly to maintain a high transfer efficiency [20,21]. Besides, the range of inductive power transfer remains a principal challenge. In spite of advances in various coil designs and the capability to create spatial Bessel beams [22], it remains difficult to overcome the performance deterioration due to the poor tolerance in coil misalignment, especially in the weak-coupling regime [23,24].

Very recently, a new WPT mechanism based on the concept of parity-time (PT) symmetry incorporating a nonlinear gain-saturation element has been projected to address this long-existing challenge [7]. Specifically, this system is engineered to have a subtle balance of energy flowing in (i.e., gain) and out (i.e., loss), and in its exact PT-symmetric phase, a nearly perfect transfer efficiency that is independent of the coupling strength can be achieved for the short-range operation. Even more importantly, this PT-symmetric nonlinear WPT system does not need the dynamic frequency reconfiguration. In contrast, when the standard second-order PT system is adopted for wireless powering applications [7], the system requires adaptive frequency tuning (although within a narrow range) and switch-mode amplifiers that cover the full range of operating frequencies. Adjusting the operating frequency may increase the design complexity and cost, since the system requires tunable filters with high quality factor and synchronization of convertor/invertor in the transmitter and receiver.

However, in the standard (second-order) PT-symmetric electronic systems [25–34], the exact PT-symmetric phase requires a moderately strong coupling strength [25,28], and this makes the system fail to maintain a satisfactory efficiency at weak/loose coupling (e.g., midrange power transfer). In addition, perturbing the load resistance of receiver could lead to a symmetry-breaking phase transition [29,34] and a low efficiency is obtained in such broken PT-symmetric phases.

In the following, we will present a new nonradiative WPT system with high-order PT symmetry, as shown in Fig. 1,

---

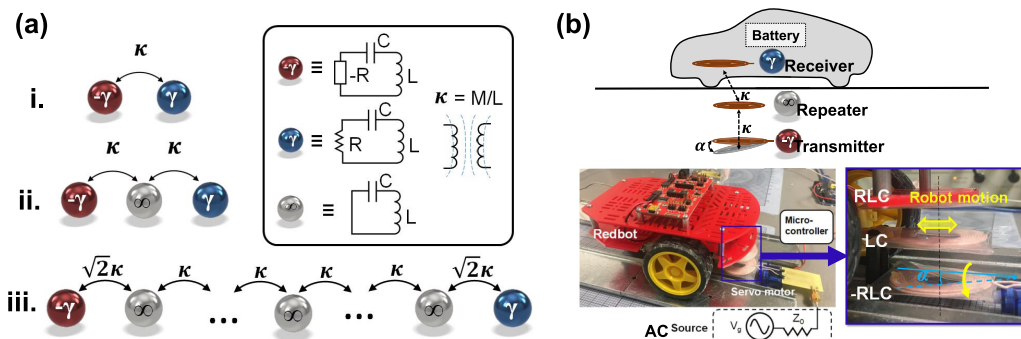*Corresponding author: pychen@uic.edu

FIG. 1. (a) Schematics for (i) standard, (ii) third-order, and (iii) generalized higher-order PT-symmetric electronic systems consisting of electronic molecules with gain (red), neutral (gray), and loss (blue) properties. (b) Third-order PT-symmetric wireless power transfer system, where a robot car (loss) is wirelessly charged by a platform consisting of a repeater (neutral) and an active transmitter (gain). The inductive coupling strength between the intermediate and receiver coils (κ) is random, and that between the transmitter and intermediate coils (κ') is tuned by rotating the transmitter coil and a feedback algorithm, such that $\kappa = \kappa'$ and PT symmetry is preserved.

which can further overcome the drawback of the standard PT-symmetric WPT system. Higher-order PT-symmetric electronic systems in Fig. 1(a) exhibit a unique eigenspectral feature: a purely real eigenfrequency that is insensitive to variations in the coupling strength and the gain-loss parameter (related to the receiver's load impedance). Such a property can ensure a transfer efficiency approaching 100% over a wide range of distances and misalignment levels, thereby offering an unprecedented robustness and freedom in wireless charging.

II. HIGHER-ORDER PT-SYMMETRIC WIRELESS POWERING

In 1998, Bender and Boettcher introduced a class of non-Hermitian Hamiltonians [35] satisfying PT symmetry. Counterintuitively, if a quantum system is invariant under the combined action of space inversion ($\mathcal{P}$) and time reversal ($\mathcal{T}$), it exhibits either entirely real eigenspectra or complex conjugate eigenvalue pairs. Although PT-symmetry was originally considered as one of interesting theoretical findings in quantum physics, it has been experimentally demonstrated in opti-

cal [36,37], acoustic [38] and electronic [25–34] platforms, and has aroused intense interest for real-life applications, such as lasers [39–41], sensors [28–32,42–46], cloaks [47,48], and nonreciprocal devices [49]. In electronics, the lumped-element circuitry could be the simplest possible configuration for observation of exotic physics of PT-symmetric Hamiltonian [30]. In analogy to optical cases, spatially-distributed, balanced gain and loss can be readily realized with an active negative-resistance converter [50,51] and a resistor, which are connected through either capacitive or inductive links, as illustrated in Fig. 1(a). Figure 1(b) presents the proposed third-order (TO) PT-symmetric WPT systems with an equivalent circuit model shown in Fig. 1(a) (type ii). In this case, the transmitter, repeater, and receiver are represented by the $-RLC$, LC, and RLC oscillators, respectively. Here, inductive couplings between the neighboring oscillators are identical, and the coupling between the transmitter and receiver is assumed to be ignorable. These coupled the $-RLC$, LC, and RLC oscillators are analogous to "electronic" molecules with gain, neutral, and loss characteristics, whose relations can be described by a PT-symmetric Hamiltonian. Applying Kirchhoff's laws to this circuit, the system can be described by Liouvillian formalism:

$$\mathcal{L}\Psi = \frac{d\Psi}{d\tau}, \quad \mathcal{L} = \begin{pmatrix} 0 & 0 & 0 & 1 & 0 & 0 \\ 0 & 0 & 0 & 0 & 1 & 0 \\ 0 & 0 & 0 & 0 & 0 & 1 \\ -\frac{1-\kappa^2}{1-2\kappa^2} & \frac{\kappa}{1-2\kappa^2} & -\frac{\kappa^2}{1-2\kappa^2} & \frac{1}{\gamma}\frac{1-\kappa^2}{1-2\kappa^2} & 0 & -\frac{1}{\gamma}\frac{\kappa^2}{1-2\kappa^2} \\ \frac{\kappa}{1-2\kappa^2} & -\frac{1}{1-2\kappa^2} & \frac{\kappa}{1-2\kappa^2} & -\frac{1}{\gamma}\frac{\kappa}{1-2\kappa^2} & 0 & \frac{1}{\gamma}\frac{\kappa}{1-2\kappa^2} \\ -\frac{\kappa^2}{1-2\kappa^2} & \frac{\kappa}{1-2\kappa^2} & -\frac{1-\kappa^2}{1-2\kappa^2} & \frac{1}{\gamma}\frac{\kappa^2}{1-2\kappa^2} & 0 & -\frac{1}{\gamma}\frac{1-\kappa^2}{1-2\kappa^2} \end{pmatrix}, \tag{1}$$

where $\Psi \equiv (q_1, q_2, q_3, \dot{q}_1, \dot{q}_2, \dot{q}_3)^T$, q_k and $\dot{q}_k$ correspond to the charge stored on the capacitor and the displacement current in the kth oscillator (the subscripts 1, 2, and 3 denote the active, neutral, and passive tanks, respectively), $\tau \equiv \omega_0 t$, the natural frequency of the neutral LC tank, the gain-loss parameter (or non-Hermiticity) $\gamma = R^{-1}\sqrt{L/C}$, the coupling strength characterized by the rescaled mutual inductance $\kappa = M/L$, $\omega_0 = 1/\sqrt{LC}$, and all (angular) frequencies are

measured in units of ω_0. The effective Hamiltonian can be written as $H_{\text{eff}} = i\mathcal{L}(H_{\text{eff}}\Psi = i\partial_\tau\Psi)$, which is non-Hermitian ($H_{\text{eff}}^\dagger \neq H_{\text{eff}}$) and symmetric with respect to the PT transformation, namely $[\mathcal{PT}, H_{\text{eff}}] = 0$, with

$$\mathcal{P} = \begin{pmatrix} \mathbf{J} & 0 \\ 0 & \mathbf{J} \end{pmatrix} \quad \text{and} \quad \mathcal{T} = \begin{pmatrix} \mathbf{I} & 0 \\ 0 & -\mathbf{I} \end{pmatrix}\mathcal{K}, \tag{2}$$
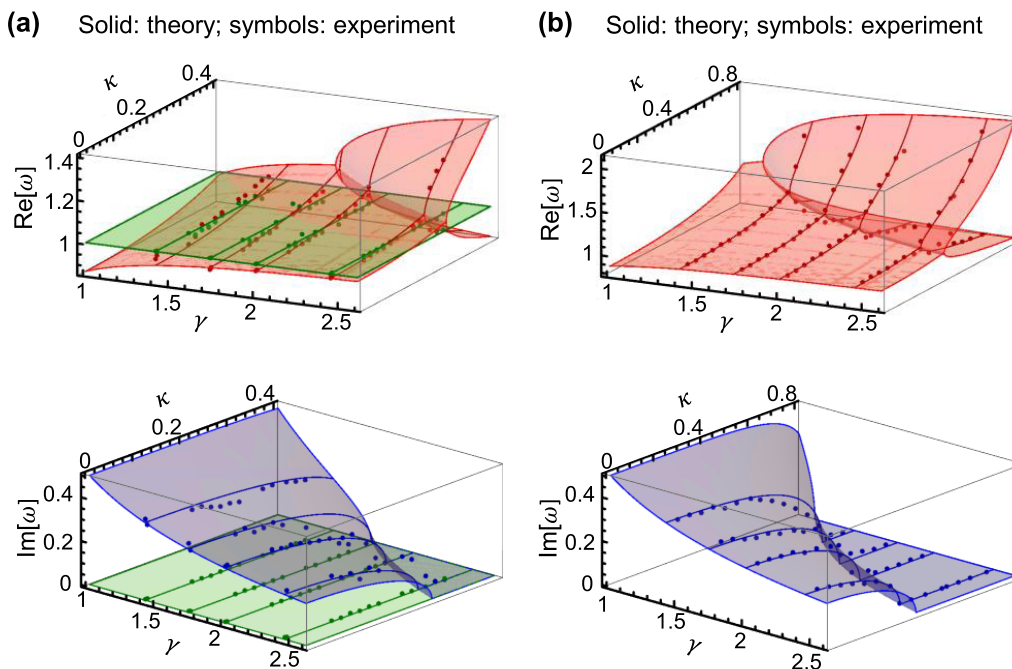
FIG. 2. Evolution of the real (top) and imaginary (bottom) parts of eigenfrequencies as a function the gain-loss parameter γ and the coupling strength κ, for the (a) third-order and (b) standard PT-symmetric electronic systems in Fig. 1(a) (see types i and ii).

where **J** is an 3×3 antidiagonal identity matrix, and $\mathcal{K}$ conducts the operation of complex conjugation. These operations in conjunction leave the system unaltered. The system has six eigenvalues or eigenfrequencies, which can be derived from the secular equation as (in units of ω_0):

$$\omega_{1,2} = \pm 1,$$

$$\omega_{3,4} = \pm \sqrt{\frac{2\gamma^2 - 1 - \sqrt{1 - 4\gamma^2 + 8\gamma^4 \kappa^2}}{2\gamma^2(1 - 2\kappa^2)}}, \quad \text{and}$$

$$\omega_{5,6} = \pm \sqrt{\frac{2\gamma^2 - 1 + \sqrt{1 - 4\gamma^2 + 8\gamma^4 \kappa^2}}{2\gamma^2(1 - 2\kappa^2)}}. \quad (3)$$

The corresponding eigenmodes can be expressed in the form of $\Phi_n = (a_n e^{-i\phi_n}, b_n e^{i\phi'_n}, a_n e^{i\phi_n}, -i\omega a_n e^{-i\phi_n}, -i\omega b_n e^{i\phi'_n}, -i\omega a_n e^{i\phi_n})^{\mathrm{T}}$, where $a_n, b_n \in R$. The dynamics (temporal response) of the PT system is the linear combination of all eigenmodes, yielding $\Psi(\tau) = \sum_{n=1}^{6} c_n \Phi_n e^{-i\omega_n \tau}$ where the coefficient c_n depends on the initial conditions. By inspecting Eq. (3), one can identify three different regimes, separated by the exceptional points $\gamma_{\mathrm{EP},\pm} = \sqrt{1 \pm \sqrt{1 - 2\kappa^2}}/(2\kappa)$. First, when $\gamma \in [\gamma_{\mathrm{EP},+}, \infty]$, the eigenfrequencies are real ($\omega_n \in R$) and $\mathcal{PT}\Phi_n = \Phi_n$ such that the *PT* symmetry is exact. When $\gamma \in [\gamma_{\mathrm{EP},-}, \gamma_{\mathrm{EP},+}]$, the eigenfrequencies become complex conjugate pairs ($\omega_n \in C$), signaling a transition to the broken phase where $\mathcal{PT}\Phi_n \neq \Phi_n$. Finally, when $\gamma < \gamma_{\mathrm{EP},-}$, all eigenfrequencies become purely imaginary. In time-transient responses, one may observe an oscillatory motion that consists of the superposition of all harmonics. In the broken phase, due to the positive imaginary part of complex eigenfrequencies, the eigenmodes grow exponentially in time, and, thus, the system exhibits an unstable, underdamped behavior. Beyond the point of critical

damping ($\gamma_{\mathrm{EP},-}$), modes are either exponentially growing or decaying eigenmodes in time. Such a phase is referred to an overdamped mode, with exponential responses arising in the temporal dynamics of charges and displacement currents.

We note that the eigenfrequencies, $\omega_{1,2} = \pm 1$, are locked to the natural frequency of the *LC* tank and are independent of κ and γ in the eigenspectrum, as can be seen in Fig. 2(a); the corresponding eigenmodes also do not experience the PT phase transition. If a TO-PT circuit is exploited to build a WPT system, the coupling-invariant, real eigenfrequency ensures the robust and stable wireless charging without hopping the operating frequency. In this system, high-efficiency power transfer always takes place at ω_0, and the performance is rather insensitive to the offset between the receiver and the transmitting module (i.e., κ variations) and to changes in the receiver's load impedance (which causes γ variations). We note that such a dark-mode behavior is not found in the standard PT-symmetric system [Fig. 2(b)] whose eigenfrequencies are always a strong function of κ and γ [25–31,52].

If a signal generator with periodically varying electromotive force is connected to the TO-PT circuit, the forced oscillations arise in the system. In the WPT case, a continuous-wave RF source (steady-state time-harmonic excitation) is connected to the $-RLC$ oscillator (transmitter). In the normal-mode analysis, an ac source with generator impedance $Z_0[\Omega]$ can be seen as a negative resistance, $-Z_0$. This is because while a positive resistor causes energy dissipations, a negative resistor represents an energy source. Therefore, if the signal generator is connected to a series $-RLC$ tank, a negative-resistance converter (NRC) with an equivalent resistance of $-(R-Z_0)$ must be used to maintain the gain and loss balance (which is identified as the necessary condition for PT-symmetric wave systems). After the substitution of time-harmonic charge distributions in each oscillator, $q_k = A_k e^{-i\omega\tau}$, the eigenfrequen-

cies (i.e., resonant frequencies found in the circuit's spectral response) are zeros of the polynomial equation $|H_{\mathrm{eff}} - \omega_n \mathbf{I}|$. We should note that the positive and negative frequency solutions are essentially identical. We must remove this redundancy by considering only the positive signs. From the circuit viewpoint, the input impedance looking into the $-RLC$ tank from the signal generator is given by

$$Z_{\mathrm{in}} = Z_0 \left\{ 1 - \eta + i \frac{\gamma \eta}{\omega}(\omega^2 - 1) \right.$$
$$\left. - i \frac{\gamma \eta \kappa^2 \omega^3 [\omega + i\gamma(\omega^2 - 1)]}{\omega(\omega^2 - 1) - i\gamma[\omega^4(\kappa^2 - 1) + 2\omega^2 - 1]} \right\}, \quad (4)$$

where $\eta = R/Z_0$. The reflection coefficient Γ measured at the input of the generator can be written as

$$\Gamma = \frac{Z_{\mathrm{in}} - Z_0}{Z_{\mathrm{in}} + Z_0}$$
$$= \frac{\prod_{n=1}^{6} \omega - \omega_n}{\frac{2\omega[\omega(\omega^2-1)+i\gamma(1-2\omega^2-(\kappa^2-1)\omega^4)]}{\eta\gamma^2(2\kappa^2-1)} + \prod_{n=1}^{6} \omega - \omega_n}. \quad (5)$$

where ω_n is the nth eigenfrequency of the system in Eq. (3). In the exact PT-symmetric phase, three sharp reflection dips are obtained at the real eigenfrequencies. Such a reflectionless property is attributed to the impedance matching, namely, $Z_{\mathrm{in}} = Z_0$, that is achieved at the resonant frequencies ($\omega = \omega_n$). In the broken phase, there is only one dip in the reflection spectrum, as the $\omega_n = \pm 1$ modes always exist in the TO-PT system.

The energy balance at the resonant frequency clarifies the spectral behavior of the TO-PT electronic system. At ω_n [Eq. (3)] and with its corresponding eigenmode Φ_n, the real power produced by the signal generator is given by $P_s = \frac{1}{2}|\dot{q}_1|^2(-Z_0)$ and the complex power delivered to the PT circuit is $P_{\mathrm{in}} = -P_{\mathrm{gain}} + P_{\mathrm{loss}} + 2j\tilde{\omega}[(\sum_{k=1}^{3} W_{\mathrm{m,k}} - W_{\mathrm{e,k}}) + W'_{\mathrm{m}}]$, where $\tilde{\omega} = \omega_n \omega_0$, the power gained from the negative-resistance element $P_{\mathrm{gain}} = -\frac{1}{2}|\dot{q}_1|^2(R - Z_0)$, the power dissipated by the resistor $P_{\mathrm{loss}} = \frac{1}{2}|\dot{q}_3|^2 R$, the average electric energy stored in each capacitor $W_{\mathrm{e,k}} = \frac{1}{4}\frac{|q_k|^2}{C} = \frac{1}{4}\frac{|\dot{q}_k|^2}{\tilde{\omega}^2 C}$, the average magnetic energy stored in each inductor $W_{\mathrm{m,k}} = \frac{1}{4}|\dot{q}_k|^2 L$, and the average magnetic energy stored in the coupled magnetic flux $W'_{\mathrm{m}} = \frac{1}{2}M\dot{q}_1\dot{q}_2^* + \frac{1}{2}M\dot{q}_2^*\dot{q}_3$. At the resonant frequencies [ω_n in Eq. (3)], the average magnetic and electric stored energies are equal, i.e., $\sum_{k=1}^{3} W_{\mathrm{e,k}} = \sum_{k=1}^{3} W_{\mathrm{m,k}} + W'$, and the power delivered to the load resistance $P_{\mathrm{in}} = \frac{1}{2}|\dot{q}_1|^2 Z_0^2 = \frac{1}{2}a_n^2 Z_0^2$, which is purely real. In this case, $P_{\mathrm{in}} + P_s = 0$; thus, the net transfer of energy from gain to loss reach a balance condition. The zero reflection at resonant frequencies can be explained by the fact that power extracted from an external source P_s is equal to that dissipated in the PT circuit P_{in}. This case is analogous to the conjugate matching condition with zero return loss (reflection) in an RF circuit, for which under a fixed generator impedance, the maximum power transfer occurs when the power lost in the source $|P_s|$ (which is considered as "gain" in a non-Hermitian electronic system) is equal to that delivered to the load. At the resonant frequencies ($\omega_1, \ldots, \omega_6$), the

power transfer efficiency defined as $\eta_T = P_{\mathrm{loss}}/(P_s + P_{\mathrm{gain}})$ can reach 100%.

In practical WPT applications, a multicoil scheme including more than one repeater [type iii design in Fig. 1(a)] is usually used, in attempt to increase the total transfer distance. Typically, the repeaters are passive LC resonators. The PT-symmetric WPT system can be generalized into the Nth order configuration ($N > 3$), of which the ac source (–RLC oscillator) and the receiver (RLC oscillator) are remotely coupled via N–2 neutral intermediators [Fig. 1(a)]. This multielement PT-symmetric electronic system can still be described by the Liouvillian formalism $d\Psi/d\tau = i\mathbf{H}_{\mathrm{eff}}\Psi$, where Ψ is the modal column vector of dimensionality N and $\mathbf{H}_{\mathrm{eff}}$ is the effective non-Hermitian Hamiltonian of dimensionality $N \times N$. We find that the generalized higher-order PT-symmetric circuits with an array of neutral repeaters [type iii design in Fig. 1(a)] share the same eigenfrequencies as those in Eq. (3) (see Appendix). In addition, there are $2(N - 2)$ eigenfrequencies that are independent of γ (see Appendix).

III. EXPERIMENTAL DEMONSTRATION OF WPT SYSTEM WITH THIRD-ORDER PT SYMMETRY

As a proof-of-concept demonstration, a TO-PT-symmetric WPT system was designed to wirelessly charge a robot car (Sparkfun Redbot-Arduino IDE) which has a receiver mounted underneath it, as shown in Fig. 1(b). The receiver is equivalent to an RLC resonator, of which the power taken by the ac-to-dc rectifier and battery (NH22NBP-NiMH 9V) is represented by a load resistance ($R = 50\,\Omega$). The transmitter comprising an LC tank connected to an RF source with generator impedance $Z_0 = 50\,\Omega$. In the Hamiltonian analysis for the PT circuit, since an RF source is represented by –Z_0 (gain), the transmitter can be seen as an –RLC resonator. If the load impedance is greater (smaller) than Z_0, a negative resistance element [28,29] (resistor) must be used. As shown in Fig. 1(b), the receiver and transmitter were wirelessly linked via an intermediate LC resonator. These three active, neutral and passive resonators form the TO-PT-symmetric electronic system in Fig. 1(a). The transmitter was positioned on a linear translation stage with rotating platform, of which the tilt angle can be precisely controlled by a linear actuator (servomotor SG90). In our experiment, the repeater was stationary and separated from the receiver (transmitter) coil by a center-to-center distance $d_R(d_T)$. The dc servomotor controlled by the LabVIEW-programmed provided a real-time positioning function to adjust the coupling strength between the transmitter and repeater coils, such that it is equal to the coupling strength between the receiver and repeater coils. This action ensures that PT symmetry is always preserved. We also used a control algorithm based on the pulse width modulation (PWM) method for determining the required tilt angle of the transmitter coil, in response to deviation in the alignment of receiver and repeater coils.

We first study the evaluation of complex eigenfrequencies as a function of γ and κ for the TO-PT and standard-PT (without the neutral LC repeater) circuits. Experimental and theoretical results shown in Fig. 2 are represented by the dots and isosurfaces, respectively. In all three resonators, the coil inductance $L = 15\,\mu H$, and the capacitance of ceramic
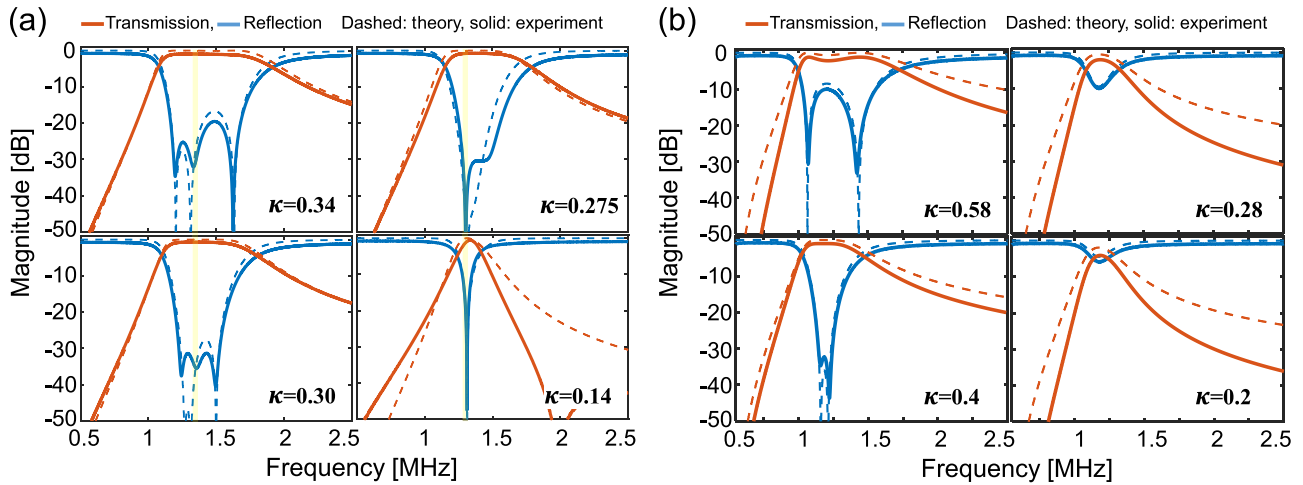
FIG. 3. Evolvement of reflection and transmission spectra for (a) the third-order PT-symmetric WPT system with the coupling strength κ varied from 0.14 to 0.34, and (b) the standard PT-symmetric WPT systems with the coupling strength κ varied from 0.2 to 0.58. Experimental and theoretical results are denoted by solid and dashed lines, respectively.

capacitors (SMA-GRM022XX series) C varies from 100 pF to 3 μF, which, in turn, varies γ from 1 to 2.5. In the receiver, the load resistance $R = 50$ Ω. The coupling strength κ varies from 0.01 to 0.77, We note that the green isosurface in Fig. 2(a) representing $\omega_1 = 1$ $[\omega_0](\omega_0/2\pi \approx 1.3$ MHz) is a flat plain in the real domain, revealing that there exists a resonance which is independent of γ and κ in the spectral response. Such an interesting characteristic is ideal for building the robust and efficient WPT systems. This nonbifurcated dark-mode is, however, not allowed in the standard PT-symmetric system [Fig. 2(b)] and all other currently existing WPT systems. The bifurcation effect is observed in both standard- and TO-PT systems, which, although can be exploited to build the $\gamma, \kappa-$ ultrasensitive wireless sensors [26–31,52], may not be suitable for wireless powering applications because the bifurcation effect demands sophisticated frequency hopping/tracking and/or adaptive impedance matching circuits.

Figures 3(a) and 3(b) report reflection and transmission coefficient versus frequency for the TO-PT and standard-PT WPT systems, respectively; here, the capacitance is fixed to 980 PF ($\gamma = 2.47$) and the coupling strenght is varied from 0.58 to 0.14 (which corresponds to a change in d_R from 20 mm to 90 mm, resulted from the software-controled motion of the robot car). In order to characterize the transmission spectrum, the transmitter and receiver were connected to cables which are attached to two ports of the vector network analyzer. From Fig. 3, we find a good agreement between theoretical [obtained with Eq. (5)] and measurement results. The experimental results show that at any arbitrary coupling strength, the transmittance (power transfer efficiency here) can be greater than 90% at frequency $\omega_0/2\pi \approx 1.3$ MHz. In contrast, the transmittance of the standard-PT WPT system drops in the weak coupling condition [see Fig. 3(b)] due to the eigenfrequency splitting effect [see Fig. 2(b)].

Finally, we compare the transfer efficiency ($\eta_T = |T|^2$) as a function of the coupling strength and the gain-loss parameter for the TO-PT and standard-PT WPT systems working at a fixed frequency. Neither system involves nonlinear gain

element [7] or frequency-tuning setup [53]. Their theoretical efficiencies are shown as red and blue isosurfaces in Fig. 4. The measurement results represented by dots in Fig. 4 agree excellently with theoretical dependency. In our experiments, the receiver capacitor was varied ($C = 100$ pF to 3 μF) and the coupling strength is tuned with respect to $d_R(\kappa = 0.01$–0.6). For the TO-PT WPT system, the resonance at $\omega_0/2\pi \approx 1.3$ MHz is invariant with respect to different PT phases. On the other hand, if a standard-PT WPT system forced to work at a given frequency, it fails to sustain a consistently high efficiency due to the bifurcation effect (which is unwanted for WPT applications). In fact, the standard-PT WPT system exhibits a high transfer efficiency only when an optimal set up of κ and γ is used (which renders an eigenfrequency equal to the operating frequency). Besides, the standard-PT setup does not function well in the weak coupling regime because of symmetry breaking that results in complex eigenfrequencies and relevant reflection. As evident from Fig. 4, our experimental results indicate that the TO-PT-symmetric arrangement can provide superior performance and
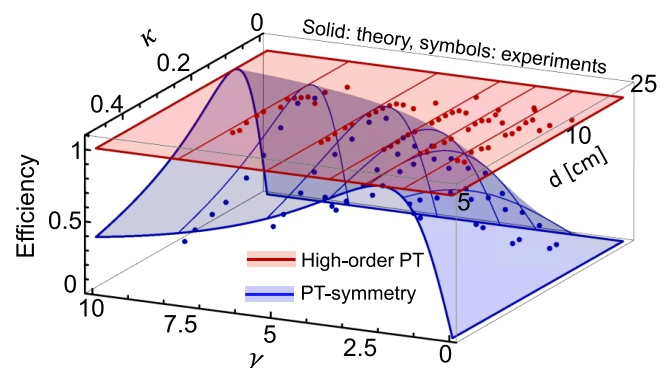

FIG. 4. Efficiency of power transfer as a function of the gain-loss parameter γ and the coupling strength κ, for the frequency-locked (1.3 MHz) standard and third-order PT-symmetric WPT systems; here d is the center-to-center distance between two neighboring coils.

better robustness compared to existing WPT systems, without any need of sweeping frequency or multistage adaptive matching stages. We should point out that the efficiency drops in the very-weak coupling regime (Fig. 4) because conduction loss that unavoidably existing in the intermediate coil [although not affecting the eigenfrequency of interet, i.e., $\text{Re}(\omega) \approx 1$] could lead to small but non-neglible imagniary parts of eigenfrequencies, and their values increase with decreasing κ. This will cause reduction of the power transmission efficiency, as can be seen in Fig. 4. Last but not least, the TO-PT WPT systems could be robust against changes in γ, associated with fluctuations in the receiver's load impedance. For example, the electrochemical fatigue or the heat damage of battery could change the load resistance or capacitance. In this case, the two bifurcating eigenfrequencies in the TO-PT circuit [see Fig. 2(a)] can be exploited for monitoring the receiver's status (i.e., by measuring the resonance shift [26–34]) and the battery lifetime. This unique feature combining simultaneous wireless charging and sensing may pave a promising new route towards the next generation of WPT systems. This technique could also benefit various industrial and medical applications, such as microwave ablation, hyperthermia, and cancer therapy, in which knowing the time-varying γ caused by physical forces (e.g., temperature or pressure) or chemical reaction during the transmission of electrical power is very important.

IV. CONCLUSION

We have shown that a real and constant eigenfrequency in the higher-order PT-symmetric electronic systems can be exploited to realize a robust wireless power transfer platform without hopping the frequency of operation. In this system, the two-dimensional eigenspectrum is flat with respect to changes in the coupling strength and the gain-loss parameter, thus ensuring a consistently high efficiency that is not influenced by distance and alignment between the receiver and the power supplier [which comprises both transmitter and repeater(s)]. Additionally, this effect is prominent even for the midrange wireless power transfer with loose magnetic coupling. The third-order PT circuit described here also exhibits bifurcating eigenfrequencies, which, together with the invariant and real one (of interest for WPT applications), may enable a multifunctional platform that simultaneously provides wireless charging and sensing. Further studies may make a breakthrough in dynamic and alignment-free wireless charging technology with extended range.

ACKNOWLEDGMENT

APPENDIX A: GENERALIZED THEORY FOR HIGHER-ORDER PT WPT SYSTEMS

Here, we consider the generalized higher-order PT-symmetric electronic system, which comprises an $-RLC$ oscillator and an RLC oscillator that are remotely coupled via N–2 neutral intermediators ($n > 3$), as shown in Fig. 1(a)

(type iii). Such a multistate scheme is also commonly seen in practical WPT applications, attempting to increase the transfer distance between the power supplier and receiver. This multielement PT-symmetric system can still be described by the Liouvillian formalism $d\Psi/d\tau = i\mathbf{H}_{\text{eff}}\Psi$, where Ψ is the modal column vector of dimensionality N and $\mathbf{H}_{\text{eff}}$ is the effective non-Hermitian Hamiltonian of dimensionality $N \times N$. Specifically, by setting the coupling strength between two neutral intermediators as κ, and that between the gain (loss) oscillator and its neighboring repeater as $\kappa' = \kappa\sqrt{2}$, the eigenvalues of $\mathbf{H}_{\text{eff}}$ can have the explicit formula obtained by means of the recurrence relation, similar to the Chebyshev polynomials. Specifically, the eigenvalues are found to be roots of the following transcendental equations:

$$(x^2 - 4\kappa^2)V_\alpha^{\text{even}} = 0 \quad \text{and} \quad \alpha = \frac{n-2}{2},$$

$$\text{for} \quad n = 4, 6, 8, \dots$$

$$(\omega^2 - 1)(x^2 - 4\kappa^2)V_\alpha^{\text{odd}} = 0 \quad \text{and} \quad \alpha = \frac{n-3}{2},$$

$$\text{for} \quad n = 5, 7, 9, \dots, \tag{A1}$$

where

$$V_\alpha^{\text{even}} = \prod_{\beta=0}^{\alpha-1} x' - (2\kappa A_{\alpha\beta})^2,$$

$$V_\alpha^{\text{odd}} = \prod_{\beta=0}^{\alpha-1} x' - (2\kappa B_{\alpha\beta})^2,$$

$$x = \left(\frac{\omega^2-1}{\omega^2}\right)^2 + \left(\frac{1}{\gamma\omega}\right)^2, \quad x' = \left(1 - \frac{1}{\omega^2}\right)^2,$$

$$A_{\alpha\beta} = \sin\left(\frac{\pi}{2}\frac{2\beta+1}{2\alpha+1}\right), \quad B_{\alpha\beta} = \sin\left(\frac{\pi}{2}\frac{\beta+1}{\alpha+1}\right),$$

and $\beta = 0, 1, 2, \dots, \alpha - 1$. If N is an odd number, eigenfrequencies are given by

$$\omega_n = \pm 1, \quad \pm\sqrt{\frac{2\gamma^2 - 1 \pm \sqrt{1 - 4\gamma^2 + 16\gamma^4\kappa^2}}{2\gamma^2[1 - 4\kappa^2]}},$$

$$\pm\frac{1}{\sqrt{1 \pm 2\kappa A_{\alpha\beta}}}. \tag{A2}$$

If N is an even number, eigenfrequencies are given by

$$\omega_n = \pm\sqrt{\frac{2\gamma^2 - 1 \pm \sqrt{1 - 4\gamma^2 + 16\gamma^4\kappa^2}}{2\gamma^2[1 - 4\kappa^2]}},$$

$$\pm\frac{1}{\sqrt{1 \pm 2\kappa B_{\alpha\beta}}}. \tag{A3}$$

From Eqs. (A2) and (A3), we find that the multistage PT-symmetric circuits with an array of neutral repeaters exhibit the γ-dependent eigenfrequencies that are identical to those of the three-elements setup. In addition, there are $2(N - 2)$ discrete eigenfrequencies that are independent of γ. All positive eigenfrequencies are bounded in the range: $\omega_n \in [1/\sqrt{1 + 2\kappa}, 1/\sqrt{1 - 2\kappa}]$. It is interesting to note that the $\gamma-$ independent eigenfrequencies, ± 1, exist only in the higher odd-order PT-symmetric circuits, which could be of interest for wireless power transfer applications.
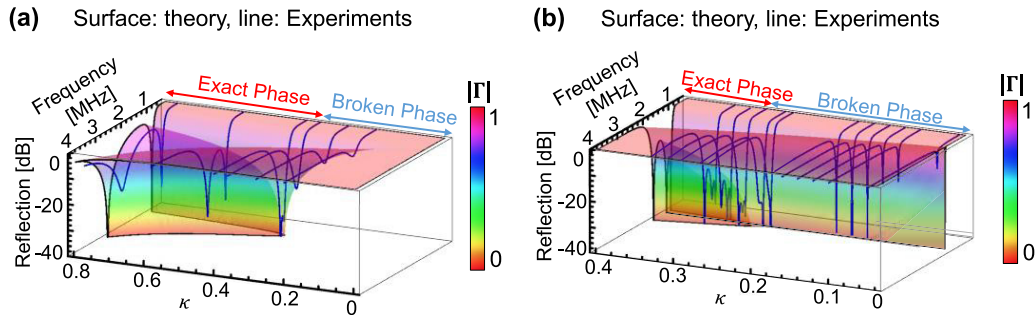
FIG. 5. Magnitude of reflection coficient as a function of frequency and coupling strength for the (a) standard and (b) third-order PT-symmetric circuits.

APPENDIX B: EVOLVEMENT OF REFLECTION AS A FUNCTION OF MAGNETIC COUPLING STRENGTH

In the exact symmetry phase of the TO-PT electronic system, $\kappa_{EP} = \sqrt{4\gamma^2 - 1}/(2\sqrt{2}\gamma^2)$ is a transition point between the exact and broken symmetry phases. Figures 5(a) and 5(b) show the experimental setup, as well as the transmission coefficient for the standard-PT and TO-PT electronic systems. In the TO-PT system, when $\kappa > \kappa_{EP}$(exact PT-symmetric phase), real eigenfrequencies lead to a near-unity transmission, and, as expected, there exists three resonant transmission peaks (or reflection dips). When $\kappa < \kappa_{EP}$(broken PT-symmetric phase), two transmission peaks associated with the bifurcating eigenfrequencies would disappear, whereas one peak locked at the same frequency is found in both exact and broken phases. This effect is, however, missed in the standard PT-symmetric system.

APPENDIX C: EFFECT OF LOSS IN THE INTERMEDIATE COIL

In a third-order WPT system, a necessary condition for PT-symmetry requires a lossless repeater (i.e., an ideal neutral

element in a Hamiltonian or Lagrangian analogue). Nevertheless, in a realistic LC resonator, conduction and dielectric loss unavoidably exists in inductive coils and capacitors. Here, we also briefly discuss the effect of loss in the repeater by assuming a loss factor $\varsigma = R'/R$, where R' and R are the equivalent resistance of the repeater and the load resistance of the receiver. Figure 5(a) presents the evolution of real parts of eigenfrequencies as a function of the coupling strength κ for $\varsigma = 0$, 0.1, and 0.2; here, the gain-loss parameter γ is fixed to 7.7. As can be seen in Fig. 6(a), loss in intermediate coil could affect the bifurcated eigenfrequencies and even makes them become complex-valued. Further, when ς increases, the real part of the nonbifurcated eigenfrequency remains insensitive to γ and κ, i.e.,$\text{Re}(\omega) \approx 1$, whereas the imaginary part starts to experience a dependency on γ and κ(not shown here). As a result, loss in the intermediate coil could affect the transmission coefficient (power transmission efficiency) at the main operating frequency ($\omega = 1$), as shown in Fig. 6(b). We should note that for the eigenfrequency of interest, its imaginary part increases with reducing the coupling strength. This may explain why the experimentally measured transmission efficiency drops in the weak coupling regime (see Fig. 4).
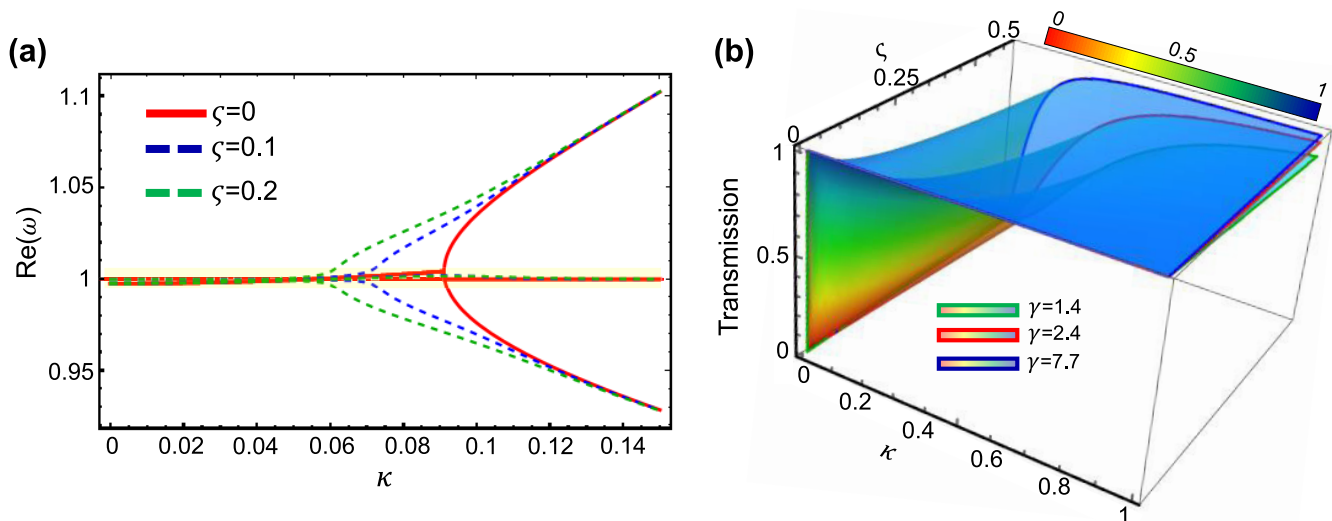

FIG. 6. (a) Evolution of real parts of eigenfrequencies as a function of the coupling strength κ for different loss factors; here, $\gamma = 7.7$. (b) Contours of the transmission coefficient as a function of the loss factors ς and the coupling strength κ at the operating frequency ($\omega = 1$).
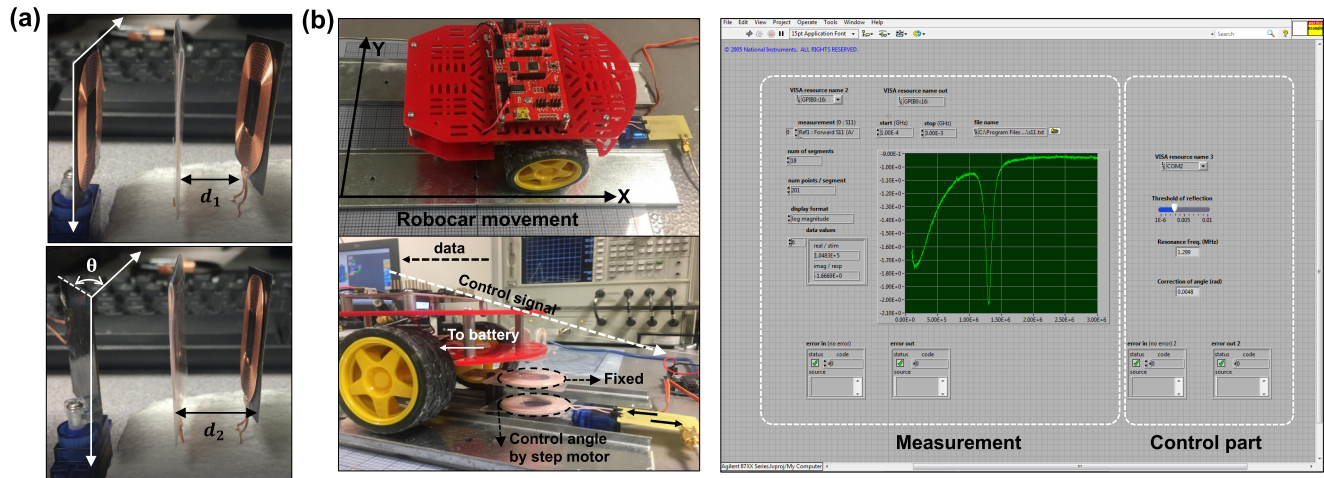
FIG. 7. (a) Control of the tilt angle of the transmitter coil by a servo motor SG90. (b) Measurment setup for the TO-PT WPT system which wirelessly charges a robot car battery (left), and the LabVIEW interface for the feedback control of rotation of the transmitter coil (right).

APPENDIX D: DYNAMIC CONTROL OF PT SYMMETRY IN CIRCUITS

The motion of the robot car (Redbot) was controlled by a pair of hobby Gearmotor-140 RPM (DG01D-A130GEARMOTOR) motorized by the H-bridge motor driver (TB6612FNG). The gearmotors was powered by a rechargeable Nickel-Metal Hydride battery (NH22NBP-NiMH 9V). The motion of robot car would change the coupling strength between the receiver coil (on the robot car) and the stationary intermediate coil. Therefore the coupling strength between the transmitter and intermediate coils must be dynamically adjusted to maintain the condition of PT-symmetry. In this work, the real-time rotation control of the transmitter coil (which alters its magnetic coupling to the repeater) was done by a dc servo motor (SG90) linked to the LabVIEW program, as illustrated in Fig. 7(a). The angle of rotation (α) for the transmitter coil is determined by the measured reflection at the resonance frequency. To this end, the relationship between the coupling strength and the reflection coefficient was mea-

sured for different values of α. In practical test environments, we first sent a PWM (Pulse Width Modulation) signal to the RF circuit and track the minimum reflection at the resonance frequency by continuously altering α. The detected reflection coefficient was used as the input of a PC-hosted peripheral LabVIEW program which contains the measurement and control modes, as shown in Fig. 7(b). In the measurement mode, the vector network analyzer (Agilent HP-8753S) as an ultrafast-switching frequency synthesizer was connected to the General Purpose Interface Bus (GPIB). The archived reflection data was dumped into the control mode as a reference for adjusting the tilt angle of the transmitter coil.

APPENDIX E: TEMPORAL RESPONSES OF THE THIRD-ORDER PT-SYMMETRIC CIRCUIT

The dynamics (time-transient response) of the TO-PT system is a linear combination of all eigenmodes
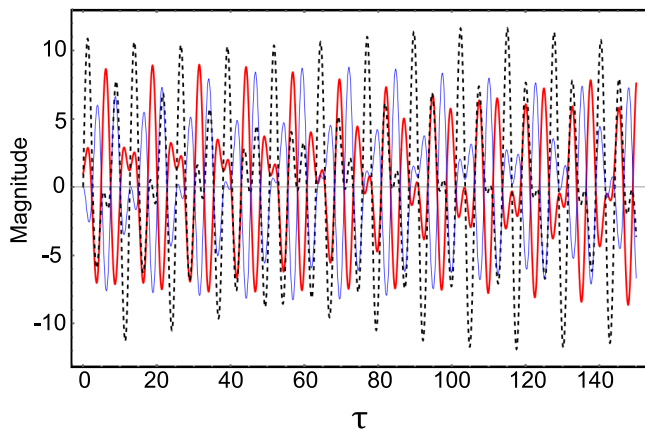

FIG. 8. **q** vs τ. Temporal dynamics of the charge stored in the capacitor of the $-RLC$ tank (red line), LC tank (black dashed line), and RLC tank (blue line); here, $\gamma = 1.5$ and $\kappa = 0.5$, which lead to the exact phase with $\omega_{1,2,3,4,5,6} = \pm 1, \pm 1.4844,$ and ± 0.9527.
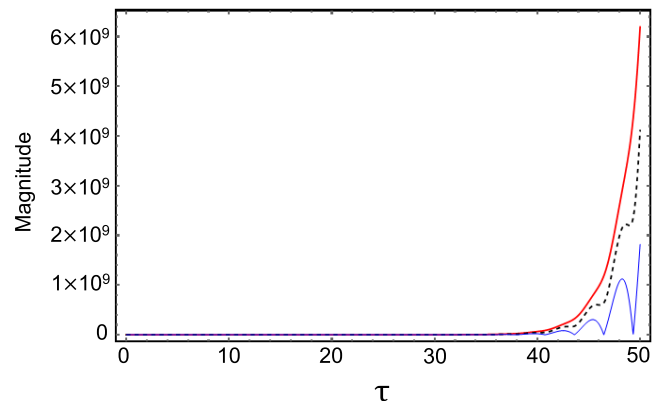
FIG. 9. $|\mathbf{q}|$ vs τ. Temporal dynamics of the absolute charge stored in the capacitor of the $-RLC$ tank (red line), LC tank (black dashed line), and RLC tank (blue line); here, $\gamma = 1$ and $\kappa = 0.5$, which renders the PT system to work in the broken phase.
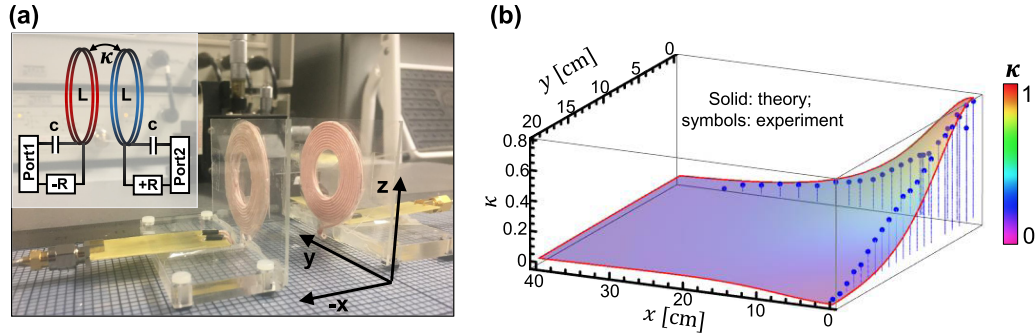
FIG. 10. (a) Measurement setup for the coupling strength between two coils. (b) Coupling strength as a function of distance (x, y); theoretical and experimental results are denoted by the isosurface and symbols.

$\Psi(\tau) = \sum_{n=1}^{6} c_n \Phi_n e^{-i\omega_n \tau}$, where the coefficient c_n depends on initial condition, and eigenfrequencies and eigenmodes can be expressed in Eq. (E1) and the following:

$$\Phi_n = (a_n e^{-i\phi_n}, b_n e^{i\phi'_n}, a_n e^{i\phi_n}, -i\omega a_n e^{-i\phi_n}, -i\omega b_n e^{i\phi'_n}, \quad -i\omega a_n e^{i\phi_n})^T, \tag{E1}$$

where $a_n, b_n \in \Box$,

$$\phi_{1,2} = \pm\pi/2,$$

$$\phi_{3,4} = \pm\frac{1}{2i} \ln\left[\frac{\kappa^2 Y_1}{\sqrt{2}(1-2\kappa^2)(Y_1 + \Delta)/Z_1 + \kappa^2(Y_1 - 4) + 2}\right],$$

$$\phi_{5,6} = \pm\frac{1}{2i} \ln\left[-\frac{\kappa^2 Z_2^2}{(1-2\kappa^2)[\sqrt{2}(Z_2 + \Delta/Z_2) - \kappa^2(Y_2 + 4) + 2]}\right],$$

$$X = \sqrt{1 - 4\gamma^2 + 8\gamma^4 \kappa^2}, \quad \Delta = 2\gamma^2(1 - 2\kappa^2),$$

$$Y_{1,2} = \pm 1 \mp 2\gamma^2 + X, \quad \text{and} \quad Z_{1,2} = \sqrt{(\pm 1 \mp 2\kappa^2)Y_{1,2}}. \tag{E2}$$

Considering for example a constant electromotive force (emf) at the initial moment $\Psi(\tau = 0) = (1, 0, 0, 0, 0, 0)^T$, the evolution of charges stored on capacitors are presented in Fig. 8.

In the *PT*-symmetric phase, one may observe an oscillatory motion that consists of the superposition of three harmonics (Fig. 8). In the broken phase, due to the positive imaginary part of complex eigenfrequencies, the eigenmodes grow exponentially in time, and, thus, the system exhibits an unstable, underdamped behavior (Fig. 9). Beyond the point of critical damping ($\gamma_{EP,-}$), the eigenfrequencies are purely imaginary and the eigenmodes are either exponentially growing or decaying in the temporal responses. Such a phase is referred to an overdamped mode, with exponential responses arising in the temporal dynamics of charges and displacement currents.

APPENDIX F: CHARACTERIZATION OF MAGNETIC COUPLING STRENGTH

We have characterized effects of vertical and horizontal misalignments on the coupling strength between coils. In our experimental setups for the third-order PT-symmetric circuits, only adjacent coils are magnetically coupled, while the coupling between nonadjacent coils is negligible. The mutual inductance between two coils can be computed using Neumann formula [24]. Figure 10 compares the theoretical and experimental results for the coupling strength (mutual inductance normalized by the coil's self-inductance). Both results are found to be in a good agreement.

[1] X. Lu, D. Niyato, P. Wang, D. I. Kim, and Z. Han, Wireless charger networking for mobile devices: Fundamentals, standards, and applications, IEEE Wirel. Commun. **22**, 126 (2015).

[2] T. Campi, S. Cruciani, F. Palandrani, V. De Santis, A. Hirata, and M. Feliziani, Wireless power transfer charging system for AIMDs and pacemakers, IEEE Trans. Microwave Theory Tech. **64**, 633 (2016).

[3] S. R. Hui, Past, present and future trends of non-radiative wireless power transfer, CPSS Trans. Power Electron. Appl., **1**, 83 (2016).

[4] C. C. Mi, G. Buja, S. Y. Choi, and C. T. Rim, Modern advances in wireless power transfer systems for roadway powered electric vehicles, IEEE Trans. Indust. Electron. **63**, 6533 (2016).

[5] S. Zhang, Z. Qian, J. Wu, F. Kong, and S. Lu, Wireless charger placement and power allocation for maximiz-

ing charging quality, IEEE Trans. Mob. Comput. **17**, 1483 (2017).

[6] H. Dai *et al.*, Safe charging for wireless power transfer, IEEE/ACM Trans. Networking (TON) **25**, 3531 (2017).

[7] S. Assawaworrarit, X. Yu, and S. Fan, Robust wireless power transfer using a nonlinear parity–time-symmetric circuit, Nature **546**, 387 (2017).

[8] T. Kan, F. Lu, T.-D. Nguyen, P. P. Mercier, and C. C. Mi, Integrated coil design for EV wireless charging systems UsingLCCCompensation topology, IEEE Trans. Power Electron. **33**, 9231 (2018).

[9] A. Triviño-Cabrera and J. A. Aguado, Wireless charging for electric vehicles in the smart cities: Technology review and impact, Transportation Power Grid Smart Cities: Communication Networks Services 411 (2018).

[10] J. Zhou, B. Zhang, W. Xiao, D. Qiu, and Y. Chen, Nonlinear parity-time-symmetric model for constant efficiency wireless power transfer: application to a drone-in-flight wireless charging platform, IEEE Trans. Indust. Electron. **66**, 4097 (2019).

[11] L. V. Bewley, *Flux Linkages and Electromagnetic Induction*, Vol. 1103 (Dover Publications, 1964).

[12] S. Nikoletseas, Y. Yang, and A. Georgiadis, *Wireless Power Transfer Algorithms, Technologies and Applications in Ad Hoc Communication Networks* (Springer, 2016).

[13] C. M. Zierhofer and E. S. Hochmair, The class-E concept for efficient wide-band coupling-insensitive transdermal power and data transfer, in *Proceedings of the 14th Annual International Conference of the IEEE Engineering in Medicine and Biology Society, Paris, France*, Vol. 2 (IEEE, 1992), pp. 382–383.

[14] Ziaie and Babak *et al.*, A self-oscillating detuning-insensitive class-E transmitter for implantable microsystems, IEEE Trans. Biomed. Eng. **48**, 397 (2001).

[15] D. Ahn and S. Hong, Wireless power transmission with self-regulated output voltage for biomedical implant, IEEE Trans. Indust. Electron. **61**, 2225 (2013).

[16] H. Dai, X. Wang, A. X. Liu, H. Ma, G. Chen, and W. Dou, Wireless charger placement for directional charging, IEEE/ACM Transactions on Networking (TON) **26**, 1865 (2018).

[17] Q. Li and Y. C. Liang, An inductive power transfer system with a high-Q resonant tank for mobile device charging, IEEE Trans. Power Electron. **30**, 6203 (2015).

[18] T.-D. Yeo, D. Kwon, S.-T. Khang, and J.-W. Yu, Design of maximum efficiency tracking control scheme for closed-loop wireless power charging system employing series resonant tank, IEEE Trans. Power Electron. **32**, 471 (2016).

[19] P. K. S. Jayathurathnage, A. Alphones, and D. M. Vilathgamuwa, Optimization of a wireless power transfer system with a repeater against load variations, IEEE Trans. Indust. Electron. **64**, 7800 (2017).

[20] S. Y. R. Hui, Magnetic resonance for wireless power transfer, IEEE Power Electronics Magazine **3**, 14 (2016).

[21] J. I. Agbinya, *Wireless Power Transfer*, Vol. 45 (River Publishers, 2015).

[22] Z. Lin, X. Li, R. Zhao, X. Song, Y. Wang, and L. Huang, High-efficiency Bessel beam array generation by Huygens metasurfaces, Nanophotonics **8**, 1079 (2019).

[23] J. O. Mur-Miranda *et al.*, Wireless power transfer using weakly coupled magnetostatic resonators, in *Proceedings of the 2010 IEEE Energy Conversion Congress and Exposition, Atlanta, GA* (IEEE, 2010), pp. 4179–4186.

[24] T. Imura and Y. Hori, Maximizing air gap and efficiency of magnetic resonant coupling for wireless power transfer using equivalent circuit and Neumann formula, IEEE Trans. Indust. Electron. **58**, 4746 (2011).

[25] J. Schindler, Z. Lin, J. M. Lee, H. Ramezani, F. M. Ellis, and T. Kottos, *PT*-symmetric electronics, J. Phys. A Math. Theor. **45**, 444029 (2012).

[26] M. Hajizadegan, M. Sakhdari, and P.-Y. Chen, PT-Symmetric inductive displacement sensors, in *Proceedings of the 2018 IEEE MTT-S International Microwave Workshop Series on Advanced Materials and Processes for RF and THz Applications (IMWS-AMP), Ann Arbor, MI* (IEEE, 2018), pp. 1–3.

[27] M. Hajizadegan, M. Sakhdari, S. Liao, and P-Y. Chen, High-sensitivity wireless displacement sensing enabled by PT-symmetric telemetry, IEEE Trans. Antennas Propag. **67**, 3445 (2019).

[28] P.-Y. Chen *et al.*, Generalized parity–time symmetry condition for enhanced sensor telemetry, Nat. Electron. **1**, 297 (2018).

[29] M. Sakhdari, M. Hajizadegan, Y. Li, M. M.-C. Cheng, J. C. Hung, and P.-Y. Chen, Ultrasensitive, parity-time-symmetric wireless reactive and resistive sensors, IEEE Sens. J. **18**, 9548 (2018).

[30] J. Schindler, A. Li, M. C. Zheng, F. M. Ellis, and T. Kottos, Experimental study of active LRC circuits with PT-symmetries, Phys. Rev. A **84**, 040101(R) (2011).

[31] P.-Y. Chen and R. El-Ganainy, Exceptional points enhance wireless readout, Nat. Electron. **2**, 323 (2019).

[32] Z. Dong *et al.*, Sensitive readout of implantable microsensors using a wireless system locked to an exceptional poin, Nat. Electron. **2**, 335 (2019).

[33] M. Sakhdari and P.-Y. Chen, Efficient and Misalignment-Robust PT-Symmetric Wireless Power Transfer, in *Proceedings of the 2019 IEEE International Symposium on Antennas and Propagation and USNC-URSI Radio Science Meeting, Atlanta, GA* (IEEE, 2019), pp. 1459–1460.

[34] M. Sakhdari, M. Hajizadegan, Q. Zhong, D. N. Christodoulides, R. El-Ganainy, and P.-Y. Chen, Experimental Observation of PT Symmetry Breaking near Divergent Exceptional Points, Phys. Rev. Lett. **123**, 193901 (2019).

[35] C. M. Bender and S. Boettcher, Real Spectra in Non-Hermitian Hamiltonians having *PT*-Symmetry, Phys. Rev. Lett. **80**, 5243 (1998).

[36] M. C. Rechtsman, Optical sensing gets exceptional, Nature (London) **548**, 161 (2017).

[37] K. G. Makris, R. El-Ganainy, D. N. Christodoulides, and Z. H. Musslimani, PT-symmetric optical lattices, Phys. Rev. A **81**, 063807 (2010).

[38] R. Fleury, D. Sounas, and A. Alù, An invisible acoustic sensor based on parity-time symmetry, Nat. Commun. **6**, 5905 (2015).

[39] Y. D. Chong, Li Ge, and A. D. Stone, PT-Symmetry Breaking and Laser-Absorber Modes in Optical Scattering Systems, Phys. Rev. Lett. **106**, 093902 (2011).

[40] L. Feng, Z. J. Wong, R.-M. Ma, Y. Wang, and X. Zhang, Single-mode laser by parity-time symmetry breaking, Science **346**, 972 (2014).

[41] M. Sakhdari, N. M. Estakhri, H. Bagci, and P.-Y. Chen, Low-Threshold Lasing and Coherent Perfect Absorption in

Generalized PT-Symmetric Optical Structures, Phys. Rev. Appl. **10**, 024030 (2018).

[42] P-Y. Chen and J. Jung, PT Symmetry and Singularity-Enhanced Sensing Based on Photoexcited Graphene Metasurfaces, Phys. Rev. Appl. **5**, 06018 (2016).

[43] H. Hodaei *et al.*, Enhanced sensitivity at higher-order exceptional points, Nature **548**, 187 (2017).

[44] W. Chen, S. K. Özdemir, G. Zhao, J. Wiersig, and L. Yang, Exceptional points enhance sensing in an optical microcavity, Nature (London) **548**, 192 (2017).

[45] M. Sakhdari, M. Farhat, and P.-Y. Chen, PT-symmetric metasurfaces: Wave manipulation and sensing using singular points, New J. Phys. **19**, 065002 (2017).

[46] J. Wiersig, Sensors operating at exceptional points: General theory, Phys. Rev. A **93**, 033809 (2016).

[47] Z. Lin, H. Ramezani, T. Eichelkraut, T. Kottos, H. Cao, and D. N. Christodoulides, Unidirectional Invisibility Induced by PT-Symmetric Periodic Structures, Phys. Rev. Lett. **106**, 213901 (2011).

[48] D. L. Sounas, R. Fleury, and A. Alù, Unidirectional Cloaking Based on Metasurfaces with Balanced Loss and Gain, Phys. Rev. Appl. **4**, 014005 (2015).

[49] H. Ramezani, T. Kottos, R. El-Ganainy, and D. Christodoulides, Unidirectional nonlinear PT-symmetric optical structures, Phys. Rev. A **82**, 043803 (2010).

[50] M. P. Kennedy, Chaos in the colpitts oscillator, IEEE Transactions on Circuits Systems **41**, 771 (1994).

[51] B. Razavi, *RF Microelectronics* (Prentice Hall, New Jersey, 1998).

[52] G. W. Hanson, A. B. Yakovlev, M. A. K. Othman, and F. Capolino, Exceptional points of degeneracy and branch points for coupled transmission lines—linear-algebra and bifurcation theory perspectives, IEEE Trans. Antennas Propag. **67**, 1025 (2019).

[53] A. Kurs, A. Karalis, R. Moffatt, J. D. Joannopoulos, P. Fisher, and M. Soljačić, Wireless power transfer via strongly coupled magnetic resonances, Science **317**, 83 (2007).